Anal. Bioanal. Electrochem., Vol. 16, No. 5, 2024, 423-437
https://www.doi.org/10.22034/abec.2024.713502

Analytical & Bioanalytical Electrochemistry

2024 by CEE
www.abechem.com

Full Paper

Electrodeposition of Copper Doped ZnO Nanotubes and Its Impact on Photoelectrocatalytic Property of ZnO Nanostructure in Improving Photoelectrochemical Water Splitting

Tahere Mollaei,[1] Ahmad Rouhollahi,[1,*] Mojtaba Hadi,[2] and Fatemeh Rasouli[1]

[1]*Faculty of Chemistry, K.N. Toosi University of Technology, Tehran, Iran*
[2]*Department of Chemistry, Faculty of Sciences, University of Qom, Iran*

*Corresponding Author, Tel.: +98-23064222
E-Mail: rouhollahi@kntu.ac.ir

Received: 13 January 2024 / Received in revised form: 5 May 2024 / Accepted: 7 May 2024 / Published online: 31 May 2024

Abstract- The ZnO nanorods, ZnO nanotubes, and Cu-doped ZnO nanotube photoanodes were electro-synthesized to improve the photoelectrochemical water-splitting performance. The structural, optical, morphologic, and photoelectrocatalytic properties of the prepared samples were investigated. UV-visible results show Cu-doped ZnO nanotube photoanode extends the visible light absorption and reduces the band gap. Mott-Schottky analysis displays that the Cu-doped ZnO nanotube sample has higher electron density than other samples. Nyquist plots indicate that Cu doping reduces the charge transfer resistance and improves charge transfer. By comparing the LSV voltammograms, it was found that Cu-doped ZnO nanotube photoelectrode has a maximum photocurrent density of 78.3 µA/cm2 at 1.6 V vs. RHE. While the value of photocurrent density obtained for pure ZnO nanorods sample is 9.6µA/cm2 at 1.6 V vs. RHE. Due to the role of Cu in reducing the band gap and reducing the charge recombination rate, Cu doping enhances the photoelectrochemical efficiency of the ZnO nanotube.

Keywords- Band gap; Cu doping; ZnO nanotubes; Water splitting; Photoanode

1. INTRODUCTION

Today, the energy crisis and environmental pollution problems have become a serious concern for mankind. Therefore, the application of clean energy is a significant challenge for

scientists. Recently, photoelectrochemical water splitting (PEC) has attracted much attention as a valuable and beneficial method for hydrogen and oxygen production [1,2]. Metal oxide semiconductors are widely used in PEC systems due to their unique characteristics and are investigated as photoanodes in these systems [3,4]. On the other hand, reports have shown that one-dimensional nanostructures are a good choice for PEC systems due to their excellent surface area and efficient charge transport [5,6]. Among the available options for choosing a photoelectrode, ZnO has gained a lot of popularity due to its excellent properties [5]. Various structures [7-11] and synthesis methods [4,12–14] have been mentioned for ZnO, which mainly use the electrodeposition synthesis method and one-dimensional ZnO nanostructure for PEC water splitting. The band gap of ZnO is wide and is about 3.2 eV, this is the factor that limits its PEC performance [15,16]. Various strategies such as heterojunction structures [17–19] and doped structures with noble metals (such as Pt, Pd, Au, and Ag) [20,21] have been performed to reduce these limitations. Heterogeneous structures require materials with appropriate energy levels and in some cases act as carrier traps and recombination centers [22,23]. Doping with metal ions reduces the band gap and recombination rate of charge carriers by creating an impurity level in the conduction band or valence band [24–26]. Cu^{2+} ions are cheaper than noble metal ions, and their ionic radius is very little different from Zn^{2+} ions, so Cu^{2+} ions are suitable for doping [24].

Herein, Cu-doped ZnO nanotubes (ZnO NTs: Cu) were prepared by electrodeposition technique, and the effect of Cu ion on the photocatalytic activity of ZnO nanotubes was investigated.

2. EXPERIMENTAL SECTION

2.1. Materials

All chemicals used were analytically graded and included Na_2SO_4, $NaNO_3$, ($Zn(NO_3)_2{\cdot}6H_2O$), acetone, 2-propanol, $CuSO_4$ and hexamethylenetetramine (HMTA). The fluorine-doped tin oxide (FTO) substrate (8-10 Ω) was bought from Nano Gostar Sepahan Company. All chemicals and reagents were purchased from Merck Company.

2.2. Preparation of ZnO nanorods, ZnO NTs and ZnO NTs: Cu

First, FTO was cleaned in three consecutive steps by immersion in 2-propanol, acetone and deionized water for 10 minutes. A three-electrode system was used to prepare photoanodes.FTO glass substrate was considered as working electrode, Pt plate as counter electrode and Ag/AgCl (3.0 M KCl) as reference electrode. The ZnO nanorod (ZnO NR) photoanode was electrodeposited from an aqueous solution containing 1.0 mM $Zn(NO_3)_2{\cdot}6H_2O$, 1.0 mM HMTA and 0.1 M $NaNO_3$ in two-step potentiostatic electrolysis. In the first step, a seed layer is formed on the FTO substrate by applying a high potential of -1.3

V for 0.5 s vs. Ag/AgCl. In the next step, a constant potential of -1.0 V vs. Ag/AgCl is applied for one hour (at a constant temperature of 80 °C). During this period, ZnO nanostructures grow vertically. Next, to prepare the ZnO NT photoanode, KOH solution with a concentration of 0.125 M and a temperature of 85 °C was used. In this way, the ZnO NR sample is immersed in this solution for 20 min and is transformed into ZnO NT during a process called etching. The electrodeposition method was also used for the synthesis of ZnO NTs: Cu photoelectrode with copper doped, with the difference that the electrolyte solution contained different concentrations of CuSO4 (4, 5 μM). Finally, the prepared samples were washed with deionized water and annealed at 300 ºC for one hour.

2.3. Characterization

The surface morphology of the semiconductors was characterized by field emission scanning electron microscope (FESEM at 15 kV). Energy-dispersive X-ray spectroscopy (EDX) was used for the chemical composition. FESEM and EDX analysis were done by a MIRA3 (Tescan Company) instrument. The crystalline phases of samples were explored by X-ray diffraction (XRD, θ/2θ) Bragg-Bentano geometry) analysis equipped with Cu Kα irradiation (λ = 1.5406 Å). The optical properties of photoanodes were measured with UV-Vis spectrophotometer (Shimadzu Company) at room temperature in the wavelength range of 350-700 nm.

2.4. PEC measurements

The PEC performance experiments of the fabricated samples were carried by linear sweep voltammetry (LSV) in 0.5 M Na_2SO_4 electrolyte. The photocurrent was measured in a three-electrode configuration connected to a potentiostat/galvanostat (Autolab PGSTAT30), where the synthesized samples was applied as working electrode, Pt plate as counter electrode and Ag/AgCl (3.0 M KCl) as reference electrode, respectively. All the measured potentials vs. Ag/AgCl were converted to the reversible hydrogen electrode scale ($E_{RHE} = E_{(Ag/AgCl)} + 0.210$ V + 0.0591 pH). The electrochemical impedance spectroscopy (EIS) measurements were performed under light and dark conditions (100 kHz to 0.1 Hz). The light source used in this work is a white LED light (100 W, λ = 500-530 nm and with an intensity of 5 mW/cm^2).

3. RESULTS AND DISCUSSION

3.1. EDX, FESEM and XRD analysis

The EDX analysis displays peaks for the elements Zn, O, Cu, and Sn (shown in Figure 1). In Figures 1a and b, the EDX spectra of ZnO NR and ZnO NT samples show that they contain only Zn and O elements. In addition to the elements mentioned, the presence of Cu element in Figure 1c confirms the formation of ZnO NTs: Cu. The appearance of Sn peak in all EDX

spectra is due to the FTO substrate constituents. The results obtained from the EDX spectra are compatible with the EDX mapping images (Figure 1d).

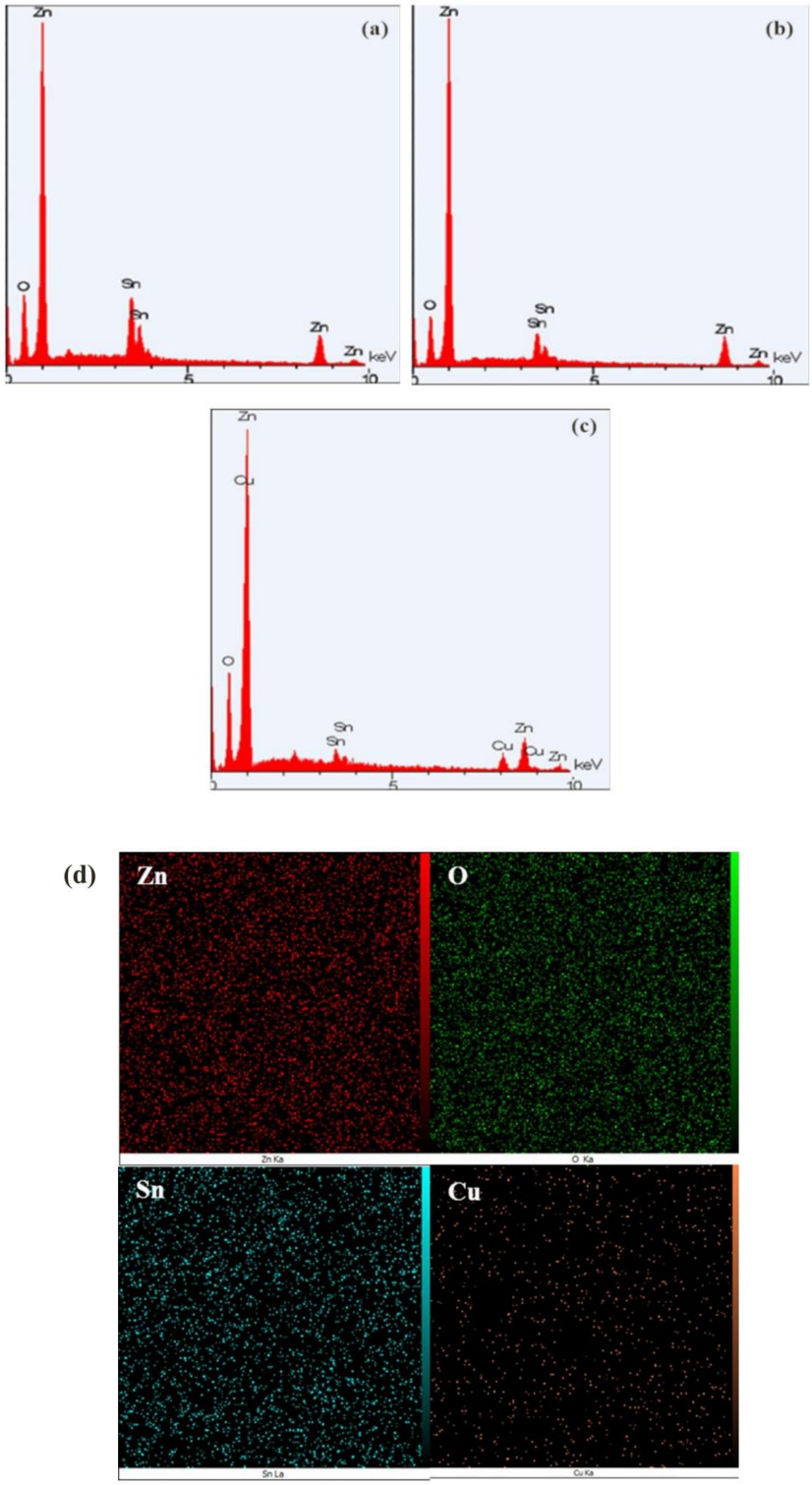

Figure 1. EDX patterns of (a) pure ZnO NRs, (b) ZnO NTs, (c) ZnO NTs: Cu and (d) EDX mapping

Figure 2 shows FESEM images of prepared films. Figure 2a displays the vertically well-aligned of ZnO NR arrays with hexagonal shapes deposited on FTO substrate. Figure 2b indicates the ZnO NTs after the etching process, showing that the opening of the tubes is well opened and completely emptied. From Figure 2c, it is clear that Cu-doped ZnO NT films have a smaller diameter than the other samples. The formation of ZnO depends on the amount of hydroxide ions produced [28] and because the concentration of hydroxide ions increases at the growth temperature above 50 °C, as a result, the growth of Cu-doped ZnO can be faster. Also, Cu ions can increase the growth rate of nanorods by increasing the density of the nucleation site during the growth process [29]. In addition, the diameter of nanotubes decreases, which is attributed to the replacement of Zn^{2+} ions by smaller Cu^{2+} ions (according to XRD results).

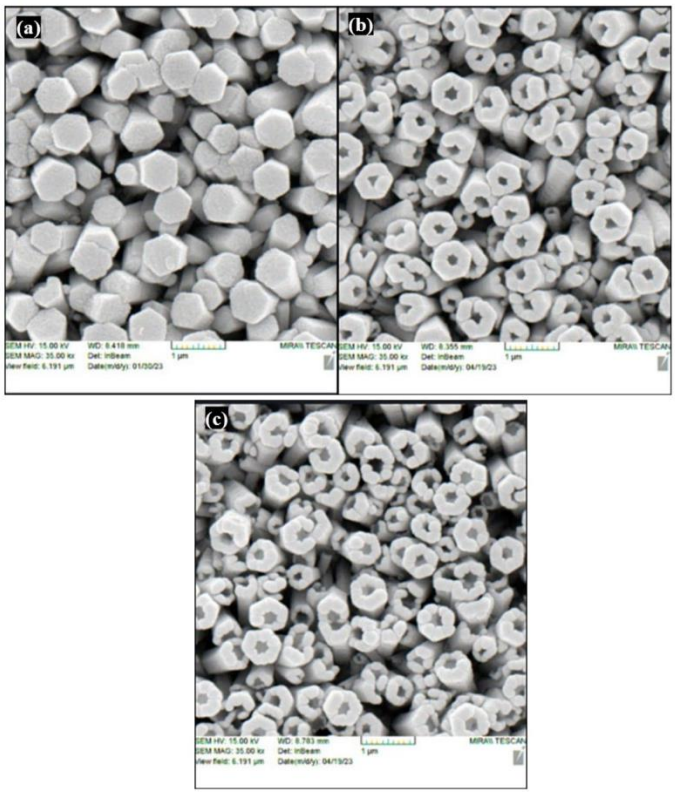

Figure 2. FESEM images of (a) pure ZnO NRs, (b) ZnO NTs and (c) ZnO NTs: Cu

The phase composition and crystallographic structure of samples deposited on the FTO substrate were examined by XRD and their XRD patterns are shown in Figure 3. The narrow and sharp XRD peaks indicate the good crystalline properties of the films. The XRD pattern of ZnO NRs in Figure 3a displaying the peaks at 2θ = 31.73°, 34.43°, 36.28°, 47.58°, 56.78°, 63.03° and 68.03° were assigned to (100), (002), (101), (102), (110), (103) and (112) planes of the hexagonal wurtzite ZnO crystal structure. These results are very close to the standard data of pure ZnO (JCPDS card number: 36-1451) [30]. The XRD pattern and peak positions of the nanotubes are similar to nanorods [31].

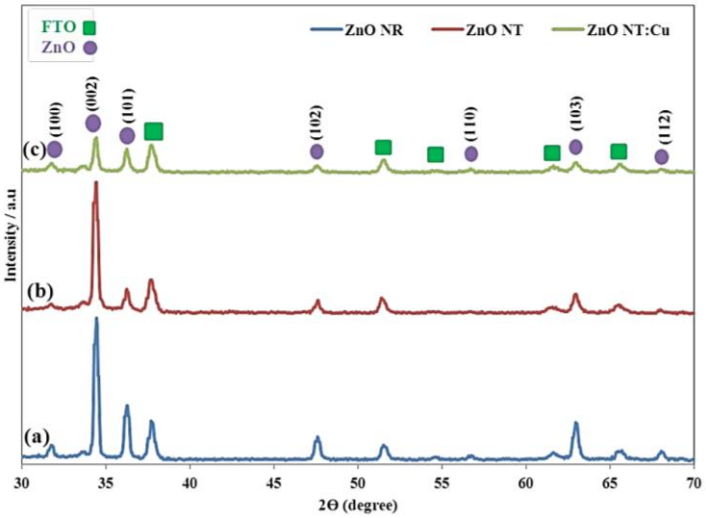

Figure 3. XRD patterns of (a) pure ZnO NRs, (b) ZnO NTs, and (c) ZnO NTs: Cu

All the films show strong (002) peaks, indicating growth along c-axis [32]. In Figure 3c, with copper doping of the sample, the intensity of the peak corresponding to the (002) plane decreases, which is due to the replacement of Zn^{2+} ions (74 p.m.) by Cu^{2+} (71 p.m.) in ZnO, which have approximately the same ionic radius [32-34]. To further study the effect of Cu doping, the following formula was used to calculate the lattice parameters [35,36]:

$$\frac{1}{d_{hkl}^2} = \frac{4}{3}\left(\frac{h^2 + hk + k^2}{a^2}\right) + \frac{l^2}{c^2} \qquad (1)$$

The values of "a" and "c" are related to the lattice constants of the unit cell and d_{hkl} is the spacing between planes for hkl indices. These values correspond to the standard data of JCPDS card number: 36-1451 and the results are listed in Table 1.

Table 1. The variation of the peak position of (002) plane, lattice parameter "a" and "c", c/a ratio of samples

Sample	2Θ (002)	Lattice parameters (Å)		c/a ratio
		a = b	c	
ZnO NRs	34.43	3.2466	5.2034	1.6027
ZnO NTs	34.44	3.2462	5.2027	1.6027
ZnO NTs: Cu	34.45	3.2451	5.2009	1.6026

According to Table 1, when ZnO is doped with Cu, the lattice parameters decrease and prove the replacement of Zn^{2+} by Cu^{2+}. The c/a ratio in the range of 1.593-1.603 is related to the ideal hexagonal wurtzite structure [37] and according to the results, Cu doping did not change the hexagonal wurtzite structure of ZnO. Also, doping leads to the reduction of the ZnO size. Using the Debye-Scherer formula, the average crystallite size was calculated and its value decreased from 563 nm for ZnO to 422 nm for the Cu-doped ZnO NTs (Zener pining) [34].

3.2. UV-visible spectra

To investigate the effect of Cu doping on the optical properties of fabricated photoelectrodes, UV–vis absorption spectroscopy was done in the wavelength range of 350-700 nm (Figure 4a). Using Cu doping, the visible absorption and the absorption edges of Cu-doped ZnO NTs shift slightly toward higher wavelengths, showing a significant redshift. The Tauc formula was used to determine the optical band gap of samples (Figure 4b) [38]:

$$\alpha h\nu = A\,(h\nu - Eg)^n \qquad (2)$$

Where α, hν, A, Eg, and n (n = 1/2 for the allowed direct band) are the absorption coefficient, the energy of the light the band gap, the constant, and an index, respectively. By extrapolating of the absorption bands to the x-axis, the values of band gaps were computed and listed in Table 2. The reduction in optical band gap with Cu doping is originated from the closely matching energy level of localized 3d electrons of doped Cu and 2p bands of O atoms. The strong d-p hybridization between Cu and O moves up the 2p orbitals of O, which can narrow the band gap [39]. Also, 3d orbital of substitute Cu^{2+} integrates a deep acceptor level at the bottom of the conduction band of ZnO, which can reduce E_g of ZnO NTs: Cu [40].

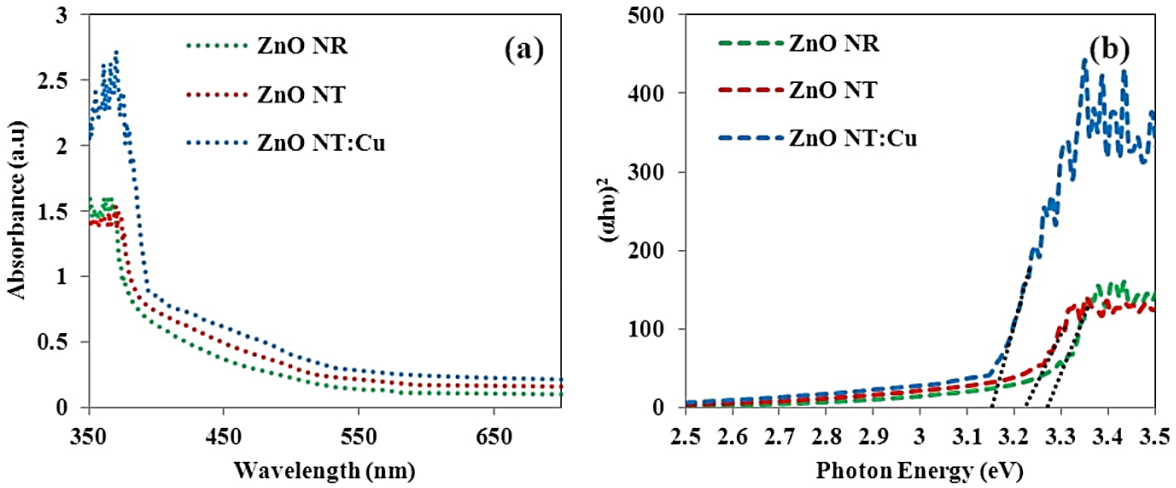

Figure 4. (a) Optical absorption spectra, (b) Band-gap of ZnO NRs, ZnO NTs ZnO and NTs: Cu

Table 2. The band gap of selected photoanodes

Sample	Band gap (eV)
ZnO NRs	3.27
ZnO NTs	3.22
ZnO NTs: Cu	3.15

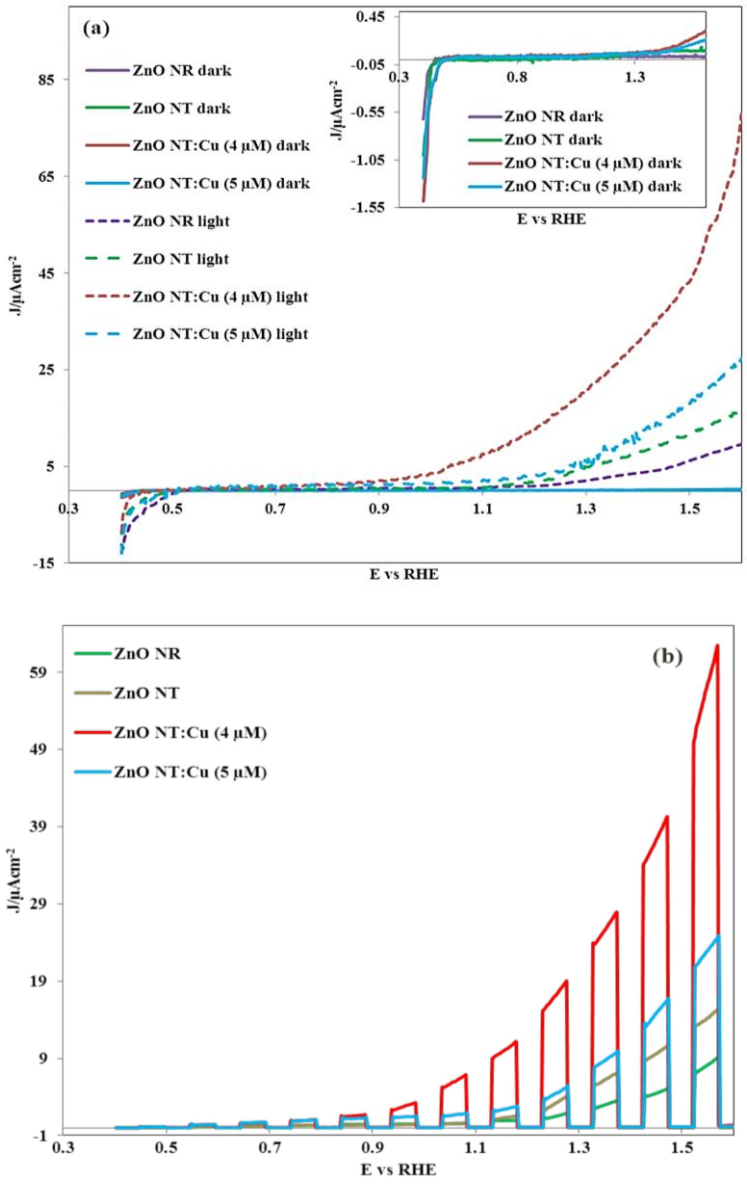

Figure 5. LSV voltammograms (a) dark and visible light conditions of ZnO NRs, ZnO NTs, ZnO NTs: Cu (4µM), ZnO NTs: Cu (5µM) in 0.5 M Na_2SO_4 solution with scan rate 5 mV/s in the potential window from 0.4 to 1.6 V vs RHE (inset during dark conditions), (b) Under chopped illumination of ZnO NRs, ZnO NTs, ZnO NTs: Cu (4µM), ZnO NTs: Cu (5µM) in 0.4 to 1.6 V vs RHE

3.3. PEC analysis of samples

To examine the PEC water splitting performance of the prepared films, LSV voltammograms were recorded in 0.5 M Na_2SO_4 electrolyte under dark and visible light conditions. Unlike dark scans that show negligible photocurrent density, the photocurrent density of semiconductors under visible light gradually increases in the desired potential range. The increase in photocurrent density in ZnO NT photoanode compared to ZnO NRs is due to the reduction of the band gap, which increases the absorption of visible light. By comparing the synthesized films, the maximum photocurrent density (78.3 μA/cm^2) at 1.6 V vs. RHE corresponds to the sample of ZnO NTs: Cu (4 μM). It is worth mentioning the increase of Cu can lead to the decomposition of the dopant phase, which acts as a carrier recombination centers, and this is the reason for the reduction of photocurrent density [41]. Also, the positivity of photocurrent density in all LSV voltammograms indicates the n-type character of the photoanodes. The increase in the photocurrent density of the doped sample and the more negative potential confirms the improvement of the photoelectrocatalytic activity. The improved PEC performance of Cu-doped photoanode is due to the role of Cu in the effective separation and transfer of charge carriers and reduced charge recombination rate.

Mott-Schottky analysis was done at a frequency of 2 kHz under darkness [42]:

$$\frac{1}{C^2} = \left(\frac{2}{e_0 \varepsilon \varepsilon_0 N}\right)\left((V_{app} - V_{fb}) - \frac{kT}{e_0}\right) \quad (3)$$

All the samples show n-type nature because the slope of all plots is positive (Figure 6). The values of carrier densities, V_{fb}, the valence band edge, and the conduction band edge of samples are reported in Table 3. ZnO NTs: Cu has a better ability to facilitate charge separation because its V_{fb} value is more negative than other samples.

Table 3. Measured flat band potential, charge carrier density, conduction, and valence band potential of selected samples

Sample	N_d (cm^{-3})	V_{fb} (V)	CB	VB
ZnO NRs	3.04×10^{21}	0.15	0.07	3.20
ZnO NTs	3.91×10^{21}	-0.03	-0.12	3.10
ZnO NTs: Cu	6.74×10^{21}	-0.11	-0.22	2.93

EIS was used to obtain kinetic information, and the resulting Nyquist curves under dark and visible light irradiation conditions are shown in Figure 7. As seen in Figure 7d, the equivalent circuit of the films composed of R_s, R_{ct} and CPE are the resistance of electrolyte

solution, the resistance of interfacial charge transfer across the electrode/electrolyte, and the constant phase element for the electrode/electrolyte interface, respectively.

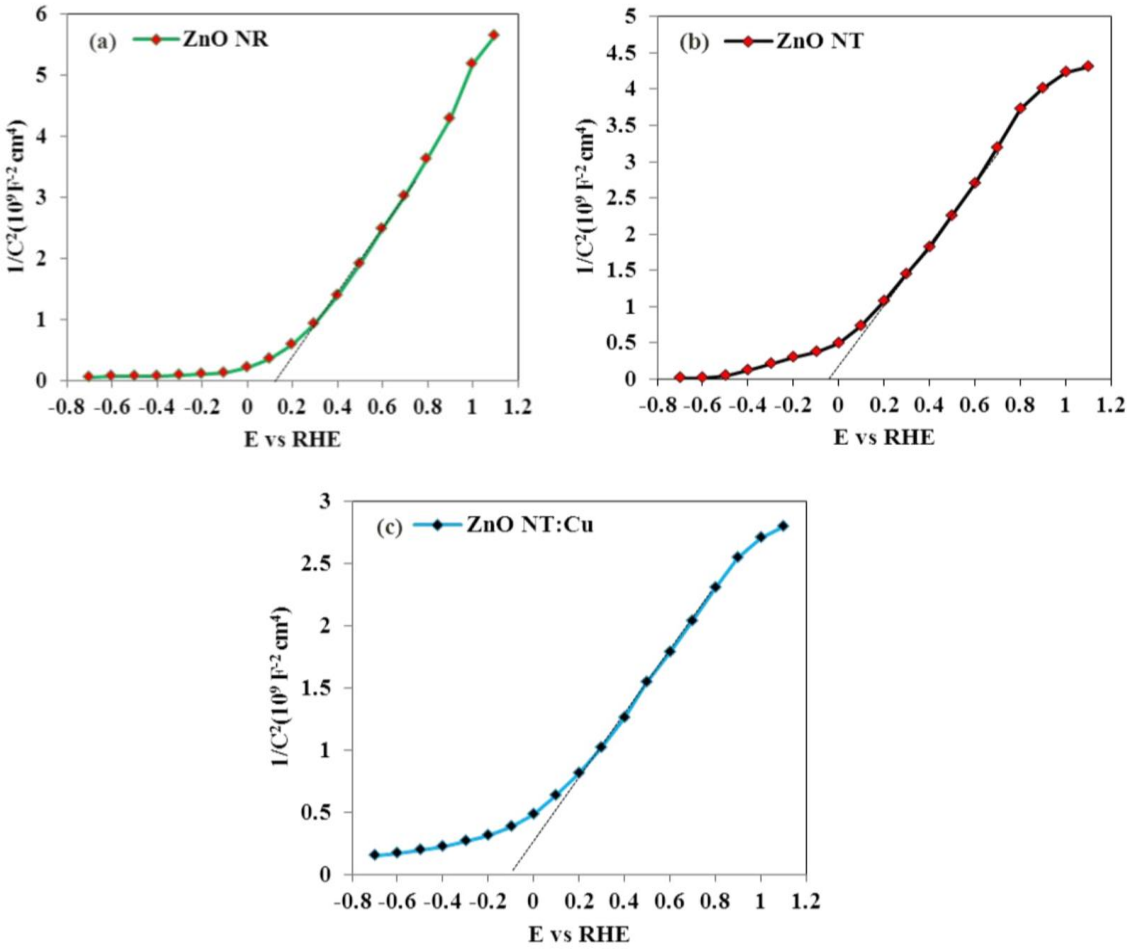

Figure 6. Mott–Schottky plots of (a) pure ZnO NRs, (b) ZnO NTs and (c) ZnO NTs: Cu NTs in 0.5 M Na_2SO_4 solution during dark conditions

Table 4. Charge transfer resistance of samples in dark and light conditions

Sample	R_{ct}/Ω dark	R_{ct}/Ω light
ZnO NRs	223.5	66.8
ZnO NTs	187.7	36.7
ZnO NTs: Cu	134.3	12.0

The semicircle part in all the curves is related to the charge transfer process (R_{ct}) and its values are listed in Table 4. EIS measurements show a significant decrease in charge transfer resistance in the ZnO NT: Cu sample (12.0 Ω) and a lower value of Rct shows a more efficient charge transfer [43].

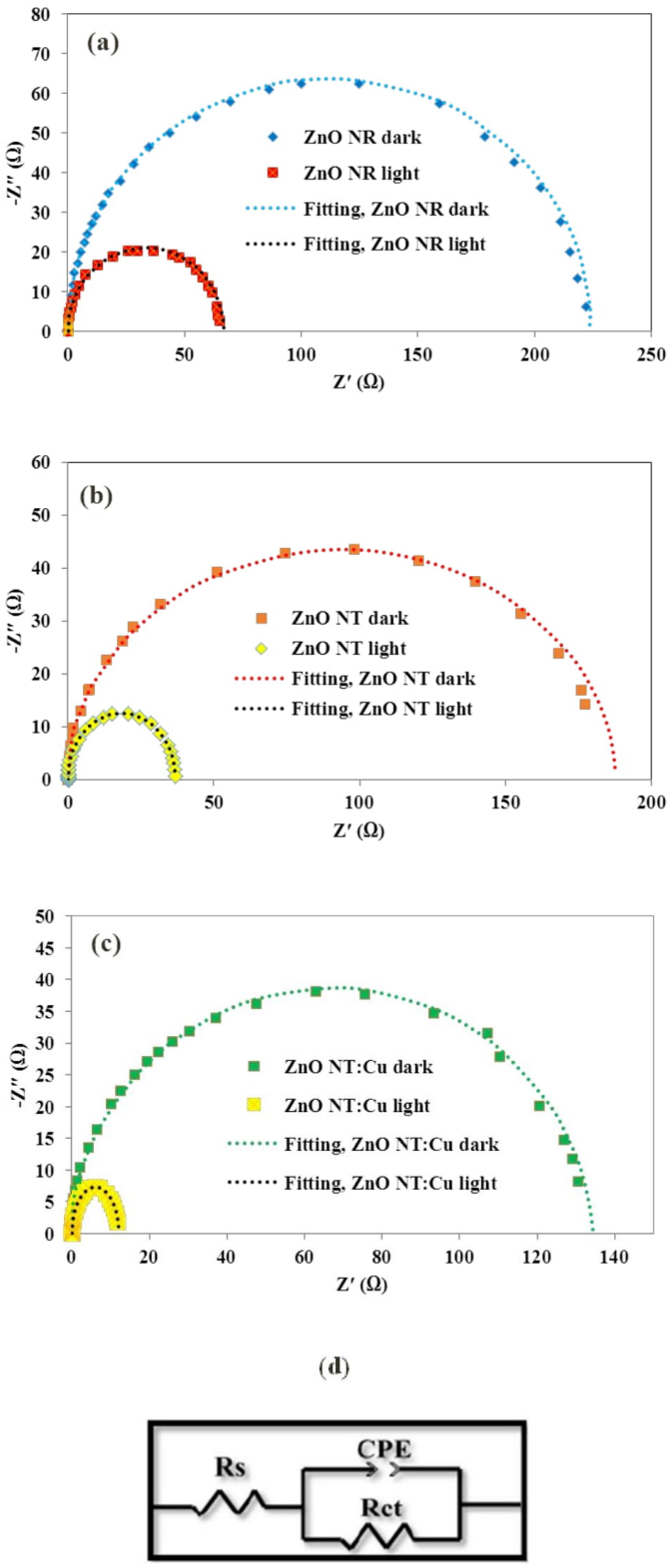

Figure 7. Nyquist plots of electrochemical impedance spectra a) pure ZnO NRs, b) ZnO NTs and c) ZnO NTs: Cu in the dark and light conditions, respectively, d) Equivalent circuits of photoanodes

Table 5 compares the present work with other reported researches.

Table 5. Comparison of the present research study with published reports including Cu and ZnO

Ref.	Method	Electrolyte	System Of Anodic	Current Density (mA cm^{-2})	Light Source
[44]	Spray pyrolysis deposition	0.5 M NaOH	Cu-doped ZnO films	0.35 (at 0.60 V vs SCE)	solar simulator (AM 1.5 G)
[45]	Ion implantation	0.5 M Na_2SO_4	Cu ion doped ZnO nanorods	0.01 (at 0.80 V vs SCE)	100 mW/cm^2 Xenon lamp
[46]	Sol-gel and spin coating	0.5 M Na_2SO_4	Cu-doped ZnO thin films	0.09 (at 0.75 V vs Ag/AgCl)	100 mW/cm^2 Xenon lamp
[47]	Two-step dc magnetron sputtering	0.5 M Na_2SO_4	ZnO films hybridized with Cu nanoparticles	0.15 (at 0.60 V vs SCE)	150 W Xenon lamp
[8]	Electrodeposition	0.5 M Na_2SO_4	Cu gradient doped ZnO nanorods	0.08 (at 0.60 V vs SCE)	5 mW/cm^2 LED
[48]	sol-gel and thermal evaporator	0.5 M Na_2SO_4	Cu-doped ZnO NRs decorated with Au NPs	0.01 (at 0.58 V vs Ag/AgCl)	150 W Xenon lamp
[49]	Electrospinning	0.1 M Na_2SO_4	Al and Cu doped ZnO thin films	0.06 (at 1.00 V vs Ag/AgCl)	100 mW/cm^2 Xenon lamp
[50]	Electrodeposition	0.1 M Na_2SO_4	Cu-doped ZnO nanorods with two different Cu precursors (Cu^{+2} and Cu^{+})	0.05 for C_2ZnO and 0.04 for C_1ZnO (at 0.20 V vs SCE)	ultraviolet lamp
This work	Electrodeposition	0.5 M Na_2SO_4	Cu-doped ZnO nanotube arrays	0. 07 (at 1.60 V vs RHE)	5 mW/cm^2 LED

4. CONCLUSION

In summary, The ZnO nanorods, ZnO nanotubes, and Cu-doped ZnO nanotube photoanodes were electro-synthesized to improve the photoelectrochemical water splitting performance. The UV-visible spectra showed that ZnO NT: Cu reduced the band gap from 3.27 to 3.15 eV. The results show that Cu doping reduces the charge transfer resistance and increases the electron density. LSV voltammograms display the maximum photocurrent density for the ZnO NT: Cu photoelectrode. The presence of Cu in the ZnO structure increases charge separation, and light absorption capacity, and reduces the charge recombination rate.

Acknowledgments

The authors gratefully acknowledged the financial support from K.N. Toosi University of Technology (KNTU) in Iran.

Declarations of interest

The authors declare that they have no known competing financial interests or personal relationships that could have appeared to influence the work reported in this paper.

REFERENCES

[1] C. Chen, W. Ma, and J. Zhao, Chem. Soc. Rev. 39 (2010) 4206.
[2] Z. Zhang, L. Zhang, M.N. Hedhili, H. Zhang, and P. Wang, Nano Lett. 13 (2013) 14.
[3] S.S. Kalanur, I.H. Yoo, and H. Seo, Electrochim. Acta 254 (2017) 348.
[4] C. Zhang, M. Shao, F. Ning, S. Xu, Z. Li, M. Wei, D.G. Evans, and X. Duan, Nano Energy 12 (2015) 231.
[5] Y. Lu, J. Zhang, L. Ge, C. Han, P. Qiu, and S. Fang, J. Colloid Interface Sci. 483 (2016) 146.
[6] N. Elamin, and A. Elsanousi, J. Appl. Ind. Sci. 1 (2013) 32.
[7] A. Kargar, K. Sun, Y.Jing, C. Choi, H. Jeong, G. Y.Jung, S. Jin, and D. Wang, ACS Nano 7 (2013) 9407.
[8] F. Rasouli, A. Rouhollahi, and F. Ghahramanifard, Superlattices Microstruct. 125 (2019) 177.
[9] Z. Li, S. Feng, S. Liu, X. Li, L. Wang, and W. Lu, Nanoscale 7 (2015) 19178.
[10] X. Ren, A. Sangle, S. Zhang, S. Yuan, Y. Zhao, L. Shi, R.L.Z. Hoye, S. Cho, D. Li, and J.L.M. Driscoll, J. Mater. Chem. A 4 (2016) 10203.
[11] A.R. Marlinda, N. Yusoff, A. Pandikumar, N.M. Huang, O. Akbarzadeh, S. Sagadevan, Y.A. Wahab, and M.R. Johan, Int. J. Hydrogen Energy 44 (2019) 17535.
[12] Z.N. Ng, K.Y. Chan, and T. Tohsophon, Appl. Surf. Sci. 258 (2012) 9604.
[13] D.N. Montenegro, A. Souissi, C. Martínez-Tomás, V. Mu˜noz-Sanjosé, and V. Sallet, J. Cryst. Growth 359 (2012) 122.
[14] X.D. Gao, F. Peng, X.M. Li, W.D. Yu, and J.J. Qiu, J. Mater. Sci. 42 (2007) 9638.
[15] S. Khanchandani, S. Kundu, A. Patra, and A.K. Ganguli, J. Phys. Chem. C 116 (2012) 23653.
[16] M. Ahmad, and J. Zhu, J. Mater. Chem. 21 (2011) 599.
[17] S.J.A. Moniz, J. Zhu, and J. Tang, Adv. Energy Mater. 4 (2014) 1301590.
[18] B.S. Shaheen, H.G. Salem, M.A. El-Sayed, and N.K. Allam, J. Phys. Chem. C. 117 (2013) 18502.
[19] J. Zhu, Z. Xu, and B. Lu, Nano Energy 7 (2014) 114.
[20] T. Wang, B. Jin, Z. Jiao, G. Lu, J. Ye, and Y. Bi, Chem. Commun. 51 (2015) 2103.
[21] Y.K. Hsu, Y.C. Chen, and Y.G. Lin, ACS Appl. Mater. Interfaces.7 (2015) 14157.
[22] M. Saad, and A. Kassis, Sol. Energy Mater. Sol. Cells.79 (2003) 507.
[23] F.F. Abdi, L. Han, A.H.M. Smets, M. Zeman, B. Dam, and R.V.D. Krol, Nat. Commun. 4 (2013) 2195.

[24] R. Saleh, and N.F. Djaja, Spectrochim. Acta Part A 130 (2014) 581.
[25] M. Pashchanka, R. Hoffmann, A. Gurlo, J. Swarbrick, J. Khanderi, J. Engstler, A. Issanin, and J.J. Schneider, Dalton Trans. 40 (2011) 4307.
[26] M. Eron, and A. Rothwarf, J. Appl. Phys. 57 (1985) 2275.
[27] F. Rasouli, A. Rouhollahi, F. Ghahramanifard, Mater. Sci. Semicond. Process 93, 371 (2019)
[28] T. Pauporté, and D. Lincot, J. Electroanal. Chem. 517 (2001) 54.
[29] A.K. Singh, G.S. Thool, R.S. Singh, and S.P. Singh, J. Alloys Compd. 618 (2015) 421.
[30] M. Ashokkumar, and S. Muthukumaran, Opt. Mater. 37 (2014) 671.
[31] A. Rokade, S. Rondiyal, V. Sharma, M. Prasad, H. Pathan, and S. Jadkar, J. Solid State Electrochem. 21 (2016) 2639.
[32] M. Wang, F. Ren, J. Zhou, G. Cai, L. Cai, Y. Hu, D. Wang, Y. Liu, L. Guo, and S. Shen, Sci. Rep. 5 (2015) 12925.
[33] Y. K. Hsu, and C.M. Lin, Electrochim. Acta 74 (2012) 73.
[34] P. Jongnavakit, P. Amornpitoksuk, and S. Suwanboon, N. Ndiege, Appl. Surf. Sci. 258 (2012) 8192.
[35] D. Raoufi, and T. Raoufi, Appl. Surf. Sci. 225 (2009) 5812.
[36] F. Ghahramanifard, A. Rouhollahi, and O. Fazlolahzadeh, Superlattices Microstruct. 114 (2018) 1.
[37] G. Sigircik, O. Erken, T. Tuken, C. Gumus, O.M. Ozkendir, and Y. Ufuktepe, Appl. Surf. Sci. 340 (2015) 1.
[38] M. Mittal, M. Sharma, and O.P. Pandey, Sol. Energy 110 (2014) 386.
[39] S.S. Xu, H.L. Lu, Y. Zhang, T. Wang, Y. Geng, W. Huang, S.J. Ding, and D.W. Zhang, J. Alloys Compd. 638 (2015) 133.
[40] K.S. Ahn, T. Deutsch, Y. Yan, C.S. Jiang, C.L. Perkins, J. Turner, and M. Al-Jassim, J. Appl. Phys. 102 (2007) 023517.
[41] X. Zhang, H. Li, S. Wang, F.R.F. Fan, A.J. Bard, J. Phys. Chem. C. 118 (2014) 16842.
[42] M. Radecka, M. Rekas, A. Trenczek-Zajac, and K. Zakrzewska, J. Power Sources 181 (2008) 46.
[43] C.Y. Lin, Y.H. Lai, D. Mersch, and E. Reisner, Chem. Sci. 3 (2012) 3482.
[44] R. Dom, L.R. Baby, H.G. Kim, and P.H. Borse, Int. J. Photoenergy (2013) 9.
[45] M. Wang, F. Ren, G. Cai, Y. Liu, S. Shen, and L. Guo, Nano Res. 7 (2014) 353.
[46] M. Salem, I. Massoudi, S. Akir, Y. Litaiem, M. Gaidi, and K. Khirouni, J. Alloys Compd. 722 (2017) 313.
[47] H. Li, X. Li, W. Dong, J. Xi, G. Du, and Z. Ji, J. Alloys Compd. 768 (2018) 830.
[48] H.Q. Huynh, K.N. Pham, B.T. Phan, C.K. Tran, H. Lee, and V.Q. Dang, J. Photochem. Photobiol. A: Chem. 399 (2020) 112639.

[49] F. Bakhtiargonbadi, H. Esfahani, R.S. Moakhar, and F. Dabir, Mater. Chem. Phys. 252 (2020) 123270.

[50] F.Z. Nouasria, D. Selloum, A. Henni, D. Zerrouki, and S. Tingry, Ceram. Int. 47 (2021) 19743.

Copyright © 2024 by CEE (Center of Excellence in Electrochemistry)

ANALYTICAL & BIOANALYTICAL ELECTROCHEMISTRY (http://www.abechem.com**)**

Reproduction is permitted for noncommercial purposes.